Noise temperature of n^+nn^+ GaAs structures

P. Shiktorov, V. Gružinskis, and E. Starikov
Semiconductor Physics Institute, Goštauto 11, 2600 Vilnius, Lithuania

L. Reggiani
Istituto Nazionale di Fisica della Materia, Dipartimento di Scienza dei Materiali, Università di Lecce, Via Arnesano, 73100 Lecce, Italy

L. Varani
Centre d'Electronique et de Micro-optoélectronique de Montpellier (CNRS UMR 5507), Université Montpellier II, 34095 Montpellier Cedex 5, France

(Received 20 March 1996)

The noise temperature of GaAs n^+nn^+ two-terminal structures of micrometer and submicrometer lengths is theoretically analyzed as a function of frequency and applied voltage. Calculations are performed at a kinetic level, and are based on a mixed Monte Carlo hydrodynamic scheme. Different operation modes of the structure are considered, namely, when operating as a nonlinear resistor (passive device) as well as when operating as a Gunn amplifier or generator (active device). Under generating conditions the noise temperature at low frequency is found to go to infinity for voltages above the threshold value for the Gunn effect, as expected in bulk material. Under amplifying conditions the noise temperature at low frequency is found to remain finite even at applied voltages well above the threshold value for the Gunn effect. At high frequencies the noise-temperature spectrum shows structures associated with transit-time effects, carrier energy, and plasma-time effects. In particular, we calculate the noise figure of merit covering both amplifying and passive conditions. Very good agreement is found between theory and available experiments. [S0163-1829(96)01634-7]

I. INTRODUCTION

One of the most used methods to investigate electronic noise in semiconductor two-terminal structures at high frequencies ($f \geqslant 1$ GHz) is the measurement of the noise-temperature spectrum $T_n(f)$. This consists of a determination of the ''black-body'' equivalent temperature under the condition that, within a given frequency bandwidth Δf centered on f, the thermal noise power generated by the black body coincides with the maximum noise power $P_{n,\max}(f)$ generated by the structure and extracted in a matched output circuit.[1] Then, by definition, it is

$$T_n(f) = \frac{P_{n,\max}(f)}{k_B \Delta f}, \tag{1}$$

where k_B is the Boltzmann constant. The dependence of T_n on an applied voltage U, doping, structure geometry, and so on is then investigated, and related to the physical processes occurring inside the structure (e.g., carrier heating, onset of intervalley transfer, appearance of negative differential conductivity, etc.).[2–5]

Despite being the direct output of a measurement, the microscopic interpretation of T_n is a difficult task, especially when the presence of sufficiently high electric fields is responsible for the onset of hot-carrier conditions. Indeed, this quantity describes the cumulative effect of two physical parameters, namely, the noise spectral density and the small-signal response of the structure, which cannot be separated without an exact knowledge of at least one of them. As a consequence, to our knowledge a detailed theoretical analysis of the noise temperature, especially when nonhomogeneous electric fields are present in the structure, is still lacking in the literature. Often it is preferred to use this quantity to obtain information about the diffusion coefficient whose interpretation has a more direct theoretical background.[6]

The aim of this work is to fill this lack of knowledge by calculating the noise-temperature spectrum of n^+nn^+ GaAs structures, eventually operating as Gunn devices, at a kinetic level. Besides providing a rigorous definition and the intrinsic limitation of this quantity, its properties will be investigated under several operating conditions of the structure. The physical implications and the possibility to provide useful figures of merits for applied purposes will be illustrated. A direct comparison of the theoretical results with available experimental data[2] will finally be carried out.

The content is organized as follows. The theoretical background and the numerical procedures for small-signal response and noise-spectra calculations are described in Sec. II. Section III presents the results obtained for the case of micron and submicron structures. Some conclusions are finally given in Sec. IV.

II. THEORY

In the following, we briefly survey the theory underlying the noise-temperature definition under far-from-equilibrium conditions, whose experimental counterpart is sketched in Figs. 1(a) and 1(b) for illustrative purposes. Figure 1(a) clearly shows the coexistence of two circuits which are used, respectively, to supply the device under test and to measure the small-signal noise whose equivalent circuit is given by Fig. 1(b).[2–5] In general, two modes of operation, voltage driven and current driven, can be used to detect electronic

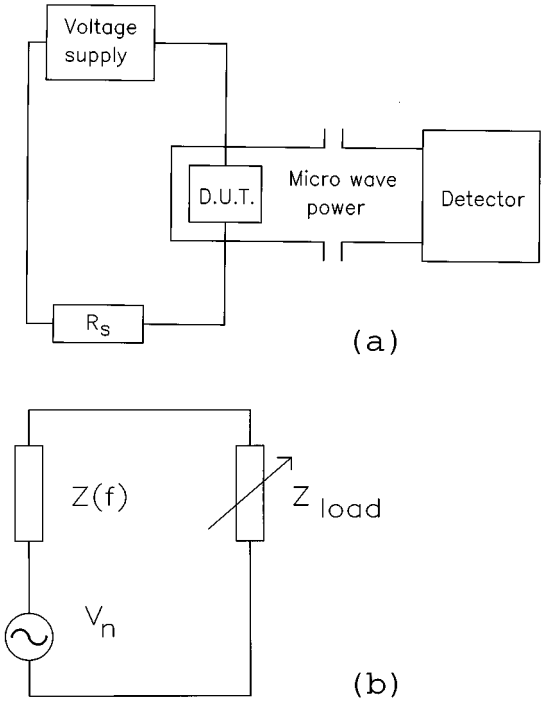

FIG. 1. (a) Schematic of the experimental setup for noise power measurements including the supplying and small-signal noise circuits. The former consists of a voltage supplier series connected with a resistance R_s and the device under test (DUT). The latter consists of the DUT placed into the waveguide, the microwave cavity, and the detector. (b) The equivalent circuit of the small-signal noise circuit which consists of the voltage-noise generator V_n connected in series with the noiseless small-signal impedance of the DUT $Z(f)$ and the load impedance Z_{load} to be tuned for matching conditions.

noise. The former is realized when the voltage drop U between the structure terminals is kept constant in time, and the fluctuating quantity is the total current I flowing through the structure. The latter is realized when the total current flowing through the structure is kept constant in time, and the fluctuating quantity is the voltage drop between the structure terminals. The supply circuit is used to choose the operation mode and to set up a working point (U,I). This consists of a constant voltage supply with a noiseless resistance R_s series connected to the device under test [see Fig. 1(a)]. Usually, in experiments[2–5] the voltage-driven operation mode is used; that is, R_s is taken to be considerably less than the device resistance. In this case, for supercritically doped Gunn devices, the onset of current self-oscillations is possible at increasing applied voltages; then the system goes to generation and a stable state is absent. In contrast, when R_s is taken to be considerably greater than the device resistance (current-driven operation mode), self-generation cannot appear for any voltage drop between the structure terminals, and the device remains in a stable state.

A theoretical description of noise is usually carried out when linear conditions with respect to fluctuations are fulfilled, and the structure remains in a stable steady state. If such a state, characterized by average values of U and I, exists in both operation modes, then the small-signal response and noise features obtained using any of these modes are equivalent. Under current-driven operation, a stable steady state is always achievable, contrary to voltage-driven operation, when the structure behaves as a generator. As a consequence, the former mode is preferable for a theoretical description of electronic noise, even if most noise experiments are performed under voltage-driven operation (or under conditions close to this mode). Our analytical analysis and numerical calculations will be carried out using mainly voltage-driven operation. Thus we will be in a position to perform a direct comparison between theory and experiments. Of course, the difference between the two modes will be stressed when this is of importance.

A. Small-signal response

Under voltage-driven operation, the small-signal response of the device at frequency f (or circular frequency $\omega=2\pi f$) is described by the small-signal admittance $Y(\omega)$. By definition, this quantity relates the linear response of the total current density at frequency ω, δj_ω to a harmonic perturbation of the applied voltage δU_ω superimposed on the steady value, so that

$$\delta j_\omega = Y(\omega)\,\delta U_\omega . \tag{2}$$

Following Shockley,[7] the calculation of $Y(\omega)$ is usually performed using a Fourier decomposition of the transient excitation.[8–10] Let a small constant perturbation of the applied voltage ΔU be superimposed to the steady value at a given initial time $t=0$. Then a transient response of the total current is calculated, and the small-signal admittance evaluated as the ratio between the corresponding Fourier components.[9] However, due to the steplike variation of the initial voltage, the transient response of the total current exhibits an initial spike, which creates some difficulties in performing numerical calculations. Since this spike is directly connected with the response of the displacement component of the total current, this problem can be overcome by considering in a separate way the conduction- and displacement-current transients. The displacement-current-density can be obtained analytically, and it makes a contribution $\omega\epsilon_r\epsilon_0/L$ to the imaginary part of $Y(\omega)$. (Here ϵ_r is the relative static dielectric constant of the semiconductor, ϵ_0 the vacuum permittivity, and L the length of the structure.) The conduction current density $j_{\text{cond}}(t)$ must be calculated numerically, and its linear-response function $K_j(t)$ is then calculated from the time derivative of the transient as

$$K_j(t)=\frac{1}{\Delta U}\frac{d}{dt}j_{\text{cond}}(t). \tag{3}$$

Finally, the small-signal admittance is obtained from the Fourier transformation of the linear-response function as[10]

$$Y(\omega)=\int_0^\infty K_j(t)\exp(-i\omega t)dt+i\omega\frac{\epsilon_0\epsilon_r}{L}. \tag{4}$$

In Eq. (4) and henceforth, $Y(\omega)$ is normalized to the cross-section area A of the device assumed to be constant throughout the structure investigated. In the calculation of transient responses, deterministic procedures, such as hydrodynamic (HD) approaches, rather than stochastic techniques, such as the Monte Carlo (MC) method, are favored because of their

better accuracy. Therefore, for small-signal calculations we shall here use a HD approach based on the continuity equation for the electron concentration, and velocity and energy conservation equations which are self-consistently coupled with the Poisson equation for the electric field. Then the stationary profiles of carrier concentration, velocity, energy, and electric field are calculated for given values of the applied voltage U. By superimposing a small constant voltage ΔU on the given value of U, the time dependence of the conduction current toward the stationary condition is obtained. Finally, from Eqs. (3) and (4), the response functions and small-signal admittance are calculated in a straightforward way. This HD approach has proven to give a rather good agreement with MC simulations for various n^+nn^+ structures up to submicrometer length scale, as reported in Refs. 11–15, where a more detailed description of the HD model and corresponding procedures can be found.

B. Current-noise spectra

The high-frequency electronic noise of typical transferred electron devices originates from velocity fluctuations of particles during their motion across the structure. In the framework of a semiclassical description based on the Boltzmann transport equation, these fluctuations are caused by carrier interactions with lattice imperfections (intravalley and intervalley phonons, impurity ions, etc.) which have a stochastic character both in time and space. The most straightforward way to take into account these fluctuations is to simulate the carrier transport through the structure with the MC method self-consistently coupled with a Poisson solver[16–18] [the so-called Monte Carlo particle (MCP) method[19]]. In accordance with the Ramo theorem,[20] for a one-dimensional geometry the instantaneous conduction current-density under constant applied-voltage conditions is given by the sum of velocities of all carriers inside the structure as[16]

$$j_{\mathrm{cond}}(t)=\frac{e}{LA}\sum_{i=1}^{N} v_i(t), \tag{5}$$

where e is the electron charge, $v_i(t)$ the instantaneous velocity of the ith particle along the direction of transport, and N the total number of particles used to simulate the carrier transport through the device. For a one-dimensional geometry and a fixed doping profile $N_D(x)$, the simulated cross section A is directly proportional to N as

$$A=\frac{N}{\int_0^L N_D(x)dx}. \tag{6}$$

In other words, the MCP simulation (including noise calculations) with N particles corresponds to the case of the ''real'' device with the cross section A defined by Eq. (6). However, the noise magnitude calculated from the simulation depends on N, thus reflecting the fact that it depends on A. Therefore, in order to compare or to use MCP results on noise together with HD calculations, one must also normalize to the unit cross section the noise features obtained by the MCP method. For this sake, one must multiply the correlation function of conduction-current fluctuations $C_j(t)$ by A. Accordingly, a multiparticle history is simulated for a time interval T sufficiently long, and $C_j(t)$ is calculated from its ergodic definition as

$$C_j(t)=\frac{A}{T}\int_0^T \delta j_{\mathrm{cond}}(t')\,\delta j_{\mathrm{cond}}(t'+t)dt', \tag{7}$$

where $\delta j_{\mathrm{cond}}(t)$ is the fluctuation of the conduction current density over its stationary value. The associated spectral density $S_j(t)$ is then obtained by the Fourier transformation as

$$S_j(f)=4\int_0^\infty C_j(t)\cos(2\pi ft)dt. \tag{8}$$

C. Noise power, noise temperature, and noise measure

The direct output of any noise experiment is the noise power which is measured by an external detector. With respect to the noise signal, the electrical properties of the whole system, which includes both the two-terminal structure and the equipment to detect its noise (detector, microwave cavity, etc.) can be represented by a small-signal equivalent circuit [see Fig. 1(b)] which contains a noise-voltage generator loaded by the complex small-signal impedance of the total circuit, $Z_{\mathrm{tot}}(f)=Z(f)+Z_{\mathrm{load}}(f)$, given by the sum of the complex small-signal impedances of the structure and the external load, $Z(f)$ and $Z_{\mathrm{load}}(f)$, respectively.[1] For such a circuit, the noise power within a frequency bandwidth Δf centered on f which is dissipated at the detector $P_n(f)$ can be related to the intrinsic characteristics of the structure and the external circuit parameters as follows. The amplitude $V_n(f)$ of the voltage noise is connected with the spectral density of voltage fluctuations $S_U(f)$ of the intrinsic diode by[1]

$$|V_n(f)|^2=S_U(f)\Delta f. \tag{9}$$

The power dissipated at the load impedance which is measured at the detector is given by

$$P_n(f)=\mathrm{Re}[U_{\mathrm{load}}(f)I^*(f)], \tag{10}$$

where

$$I(f)=\frac{V_n(f)}{[Z(f)+Z_{\mathrm{load}}(f)]} \tag{11}$$

is the current induced by the voltage-noise generator in the small-signal circuit of Fig. 1(b), and $U_{\mathrm{load}}(f)=I(f)Z_{\mathrm{load}}(f)$ is the voltage drop at the load impedance. By a combination of the above equations, one obtains

$$P_n(f)=S_U(f)\frac{\mathrm{Re}[Z_{\mathrm{load}}(f)]}{|Z(f)+Z(f)_{\mathrm{load}}|^2}. \tag{12}$$

Then, by using the standard relation between small-signal coefficients and spectral densities,

$$Z(f)=1/Y(f), \tag{13}$$

$$S_j(f)=S_U(f)/|Z(f)|^2, \tag{14}$$

Eq. (12) can be rewritten in terms of the small-signal admittance and the spectral density of current fluctuations as

$$P_n(f)=S_j(f)\frac{\mathrm{Re}[Y_{\mathrm{load}}(f)]}{|Y(f)+Y_{\mathrm{load}}(f)|^2}\Delta f=k_B T_{\mathrm{ef}}(f)\Delta f, \quad (15)$$

where, for convenience we have introduced an effective noise temperature $T_{\mathrm{ef}}(f)$ which, according to the right-hand side of Eq. (15), is defined as

$$T_{\mathrm{ef}}(f)=\frac{1}{k_B}S_j(f)\frac{\mathrm{Re}[Y_{\mathrm{load}}(f)]}{|Y(f)+Y_{\mathrm{load}}(f)|^2}. \quad (16)$$

By definition, $T_{\mathrm{ef}}(f)$ is always positive, and depends on both the intrinsic device characteristics $S_j(f)$ and $Y(f)$, and the detecting circuit parameters $Y_{\mathrm{load}}(f)$. Since the detector takes power from the structure (and not vice versa), $\mathrm{Re}[Y_{\mathrm{load}}(f)]$ is positive.

Usually $P_n(f)$ is compared to a ''black-body'' radiation of known thermodynamic temperature, which is used as a reference noise source.[2] Of course, in any experiment one is primarily interested in the intrinsic characteristics of the structure investigated. To eliminate from Eq. (16) the parameters of the detecting circuit, let us consider the variation of T_{ef} with $\mathrm{Re}[Y_{\mathrm{load}}(f)]$. The effective noise temperature of Eq. (16) is maximum when

$$\mathrm{Re}[Y_{\mathrm{load}}(f)]=[\{\mathrm{Re}[Y(f)]\}^2+\{\mathrm{Im}[Y_{\mathrm{tot}}(f)]\}^2]^{1/2}. \quad (17)$$

Substituting Eq. (17) into Eq. (16), for the maximum value $T_{\mathrm{ef,max}}(f)$, we obtain

$$T_{\mathrm{ef,max}}(f)=\frac{1}{2k_B}S_j(f)\times\frac{1}{[\{\mathrm{Re}[Y(f)]\}^2+\{\mathrm{Im}[Y_{\mathrm{tot}}(f)]\}^2]^{1/2}+\mathrm{Re}[Y(f)]}. \quad (18)$$

The physical and circuit meaning of $T_{\mathrm{ef,max}}(f)$ defined by Eq. (18) will differ according to the sign of $\mathrm{Re}[Y(f)]$. As a consequence, the following analysis will consider the sign of $\mathrm{Re}[Y(f)]$.

Passive device. In this case $\mathrm{Re}[Y(f)]>0$ for any f, and the right-hand side of Eq. (18) exhibits its maximum for $\mathrm{Im}[Y_{\mathrm{tot}}(f)]=0$. This condition corresponds to ''impedance matching,'' and the value taken by $T_{\mathrm{ef,max}}$ is called T_n, which now satisfies a generalized Nyquist relation of the form

$$T_n(f)=\frac{S_j(f)}{4k_B\mathrm{Re}[Y(f)]}. \quad (19)$$

According to Eq. (1), $T_n(f)$ is the noise temperature of the passive device, and corresponds to the maximum noise power which can be displayed at the output circuit when impedances are matched at any given applied voltage. We stress that $T_n(f,U)$ is determined by the intrinsic parameters of the device at the given applied voltage only.

Active device: amplifier. When $\mathrm{Re}[Y(f)]$ becomes negative inside a certain range of frequencies, which defines the amplification band, the two-terminal structure can be used for amplification or generation of electrical power within that band. In the case of an amplifier, the unloaded structure remains stable under constant-voltage operation;[21,22] hence $Y(f)$ is a well-defined quantity. As a consequence, outside the amplification band, one can still use Eq. (19) for a theoretical calculation of $T_n(f)$. Analogously, an experimental investigation of $T_n(f)$ is also possible since, outside the amplification band, the impedance matching can be achieved with a proper choice of the output circuit parameters. However, inside the amplification band the definition of the noise temperature given by Eq. (19) has a drawback. Indeed, negative values of $\mathrm{Re}[Y(f)]$ would imply negative values of $T_n(f)$ which, in turn, can be interpreted as the possibility for the structure to become an active element (amplifier or generator) under suitable conditions.[21,22] (In other words, negative values of $\mathrm{Re}[Y(f)]$ do not allow for an impedance matching.) To describe the noise behavior of a stable active device inside the amplification band, one can introduce the noise measure $M(f)$, a dimensionless quantity defined as[23,24]

$$M(f)=\frac{S_j(f)}{4k_B T_0\{-\mathrm{Re}[Y(f)]\}}, \quad (20)$$

where T_0 is the lattice temperature. The above quantity gives the intrinsic noise of an amplifier with a shorted input. As a rule, under voltage-driven operation the above situation is realized when the value of the nl product (here n is the doping of the n region and l its length) is sufficiently small for the self-generation to appear, and the electrical characteristics of the structure to remain stable in the whole region of applied voltage. Under current-driven operation, such a stable state of the active device can always be realized independently of the nl value, since any generation process is damped by the large external resistance of the supply circuit. Thus for this operation mode the noise-temperature and noise-measure spectra defined, respectively, outside and inside the amplification band, can be numerically calculated or experimentally measured for any value of the voltage drop between the diode terminals, including the case when U is higher than the threshold value for Gunn oscillations to appear under voltage-driven operation. For numerical calculations, in this case Eqs. (19) and (20) are used upon replacing $S_j(f)$ and $Y(f)$ with $S_U(f)$ and $Z(f)$.

Active device: generator. In this case the structure goes into the self-oscillation regime for applied voltages above a threshold value (Gunn devices). This happens when the nl product is higher than some critical value which, for GaAs Gunn devices of several micrometers length, is of about 5×10^{12} cm^{-2}. As a matter of fact, under voltage-driven operation the unloaded structure cannot achieve a stable state in the whole frequency range, as verified from both numerical simulations and experimental measurements. As a consequence, $Y(f)$ cannot be defined, and Eq. (19) fails. It should be mentioned that an intermediate situation between the amplifier and generator case can be realized for applied voltages slightly below the threshold for the Gunn effect to occur. In this situation, the structure remains stable; however, since it is very near to becoming unstable, we can expect the appearance of some extra noise source in its spectrum, as confirmed by calculations.

It should be noted that, in terms of the device's small-signal impedance $Z(f,U)$ [which, while remaining of finite magnitude, is better suited than $Y(f,U)$ for the analysis of active devices] the amplifier and generator cases differ in the sign of $\mathrm{Im}[Z(f,U)]$ inside the amplification band. When

$\mathrm{Im}[Z(f,U)]$ is negative, the structure remains stable under voltage-driven operation. When, at some frequency value inside the amplification band, $\mathrm{Im}[Z(f,U)]=0$ and $(d/df)\{\mathrm{Im}[Z(f,U)]\}>0$, the resonant condition is fulfilled, and the structure goes into self-oscillations without any external circuit.[21,22]

III. RESULTS AND DISCUSSION

We shall first consider the case of a structure operating as a Gunn generator, and sufficiently long to avoid velocity overshoot phenomena inside the n region, with the following parameters: the length of the n region is 7.5 μm, and doping concentration in the n and n^+ regions are 10^{15} and 2×10^{16} cm^{-3}, respectively. Abrupt homojunctions are assumed. The cathode and anode lengths are taken to be 0.5 μm each, which is sufficient to obtain quasi thermal-equilibrium conditions near the structure terminals. The lattice temperature T_0 is 300 K. A standard three-valley model[25] for the GaAs conduction band has been used in calculations.

To calculate the noise temperature from Eqs. (19) and (20), we use a mixed MC and HD scheme in the sense that the small-signal admittance (impedance) is obtained from HD modeling, and the current (voltage) spectral density is obtained from MCP simulations of sufficiently long histories of about $T=1$–10 ns by using $(1$–$3)\times10^4$ particles. In this way we could achieve a good accuracy for T_n, because we estimate the uncertainty to be within 1% for HD calculations and 10% for MC calculations at worst. Since HD and MCP approaches correspond to different levels of microscopic description, to check their mutual consistency we start by considering the time and frequency behavior of the response and electrical fluctuations at $U=0$. Let us recall that, under thermal equilibrium, the noise and response obey the Nyquist relation

$$S_j(f)=4k_BT_0\mathrm{Re}[Y(f)]. \tag{21}$$

Thus a comparison between the values of $S_j(f)$ obtained directly from MCP calculations and those of $\mathrm{Re}[Y(f)]$ obtained from HD calculations gives the required check of consistency.

Figure 2(a) shows the time dependence of the correlation function of current fluctuations together with the linear-response function of the current calculated from MCP and HD approaches at $U=0$ (solid and dashed lines, respectively). Both functions are normalized to their values at $t=0$. The correspondent current spectral density calculated with the MCP method and that obtained from the small-signal admittance by using Eq. (21) are presented in Fig. 2(b). Both figures clearly demonstrate the existence of an oscillatory process with a period of about 0.8 ps, and a correspondent frequency of 1.25 THz. It is the plasma frequency associated with an electron concentration of about $n=1\times10^{16}$ cm^{-3} which coincides with the value at the homojunctions. In the case of fluctuations this process leads to super-high-frequency oscillations spontaneously appearing in the time dependence of the conduction current. The oscillations are initiated by microscopic fluctuations of the carrier velocities and, hence, of the space charge at the homojunctions. Via the Poisson equation, these local fluctuations cause fluctuations of the internal electric field in the whole structure, leading to time oscillations of the total current at the plasma frequency which are observed on the macroscopic level. The spontaneous formation and destruction in time of plasma oscillations leads to the appearance of damped plasma oscillations of $C_j(t)$, as shown in Fig. 2(a). The oscillatory behavior of $C_j(t)$ implies the resonant peak in the spectral density of the current fluctuations shown in Fig. 2(b). From the excellent agreement found between results obtained with MCP and HD calculations, we conclude that both approaches give a reliable description of small-signal response and noise near thermal equilibrium.

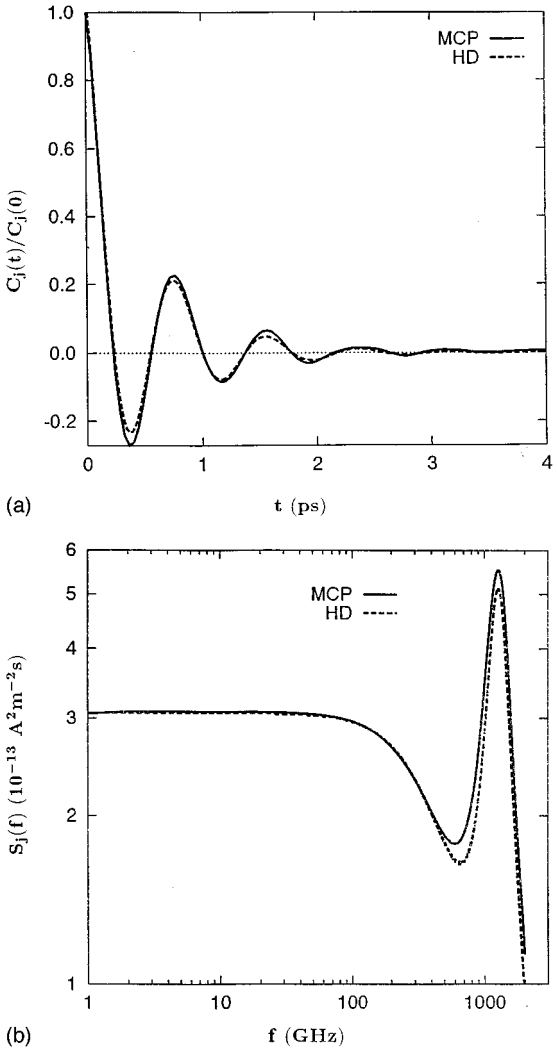

FIG. 2. (a) Time dependence of the correlation function of current fluctuations calculated with the MCP method (solid line), and of the response function of the conduction current calculated with the HD approach (dashed line) for a GaAs two-terminal n^+nn^+ structure at $T_0=300$ K and for the applied voltage $U=0$. The n- and n^+-region doping is 10^{15} and 2×10^{16} cm^{-3}, respectively; the length of the n region is 7.5 μm. Both functions are normalized to their values at $t=0$. (b) Frequency dependence of the spectral density of current fluctuations obtained by the Fourier transformation of the correlation functions presented in (a) (solid line), and by the Fourier transformation of the response function presented in (a) and using Eq. (21) (dashed line).

Figure 3 shows the current-voltage characteristic obtained with the HD and MCP approaches, and compares theory

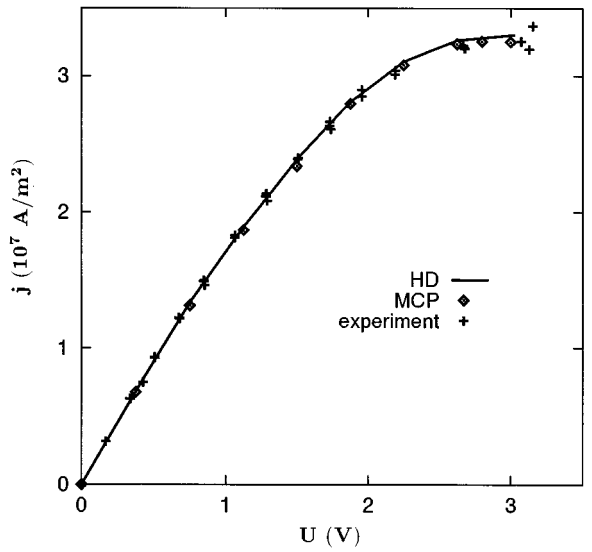

FIG. 3. Current-voltage characteristic for the n^+nn^+ GaAs structure of Fig. 2. Crosses refer to experiments, diamonds to MCP simulations, and the line to HD calculations.

with experiments.[2] The excellent agreement found validates the theoretical approach based on the mixed HD-MCP calculations also under far-from-equilibrium conditions. Both experimental and theoretical results show that the structure becomes unstable for $U>3.1$ V, where Gunn oscillations are found to appear. Therefore, the following analysis of such a generating structure is limited to voltages below this threshold value.

The electric-field and average-velocity profiles calculated with the HD approach at several values of applied voltages are shown in Figs. 4(a) and 4(b), respectively. Inside the n region, both profiles are quite flat for $U\leqslant 2.8$ V. This means that practically up to the threshold voltage carrier heating in the n region is quite homogeneous and, hence, electronic transport is quite similar to that occurring in the bulk semiconductor.

The time dependencies of the response function of conduction current calculated with the HD approach are presented on short- and long-time scales in Figs. 5(a) and 5(b), respectively. On the short-time scale, plasma oscillations similar to those at thermal equilibrium are observed. On the long-time scale, additional oscillations show up when the applied voltage approaches the threshold value. Let us recall that, by definition,[7] $K_j(t)$ describes the conduction current response to an impulsive (i.e., δ like) perturbation of the applied voltage. When U approaches the threshold value, the initial voltage perturbation leads to the formation of perturbations in carrier concentration which are similar to the usual Gunn domains. As soon as the first domain reaches the anode, a redistribution of the electric field takes place, and a second domain is formed in the n region, crosses the structure, reaches the anode, and so on. Therefore, these oscillations exhibit a transit-time character, and are connected with the successive formation and propagation of perturbations in carrier concentration through the structure. Below the threshold voltage, the gain is insufficient to support the formation of a second domain with the same amplitude as the first one, and the process of repeating transit flights is damped in time.

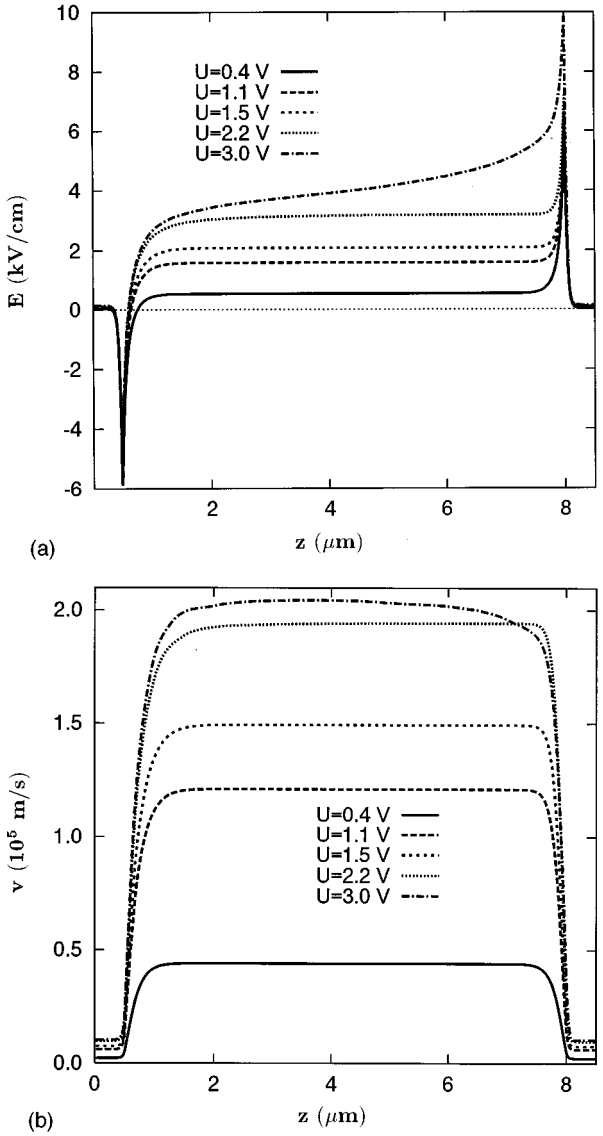

FIG. 4. (a) Electric-field and (b) drift velocity profiles calculated with the HD approach for the structure of Fig. 2 at several values of the applied voltage U.

By approaching the threshold voltage, the damping rate decreases, and the oscillations become more pronounced [see Fig. 5(b)]. At threshold, the gain becomes sufficient to support the repeating formation of Gunn domains, and the device goes to self-oscillations. Above threshold, a stationary state is absent. After some transient processes, we observe strongly periodic self-oscillations of the current in our HD modeling, and the response function defined by Eq. (3) loses its meaning. A similar behavior is observed for $C_j(t)$, as reported for short- and long-time scales in Figs. 6(a) and 6(b), respectively. Here the transit-time oscillations of $C_j(t)$ are caused by the spontaneous formation of Gunn domains and their successive displacements through the structure. Below the threshold voltage, the stochastic character of carrier velocity fluctuations (both in time and space) destroys the coherence of successive transit-time oscillations of the conduction current, and washes out their correlation on the long-time scale. By approaching the threshold, the damping rate decreases [see Fig. 6(b)], and for voltages above the

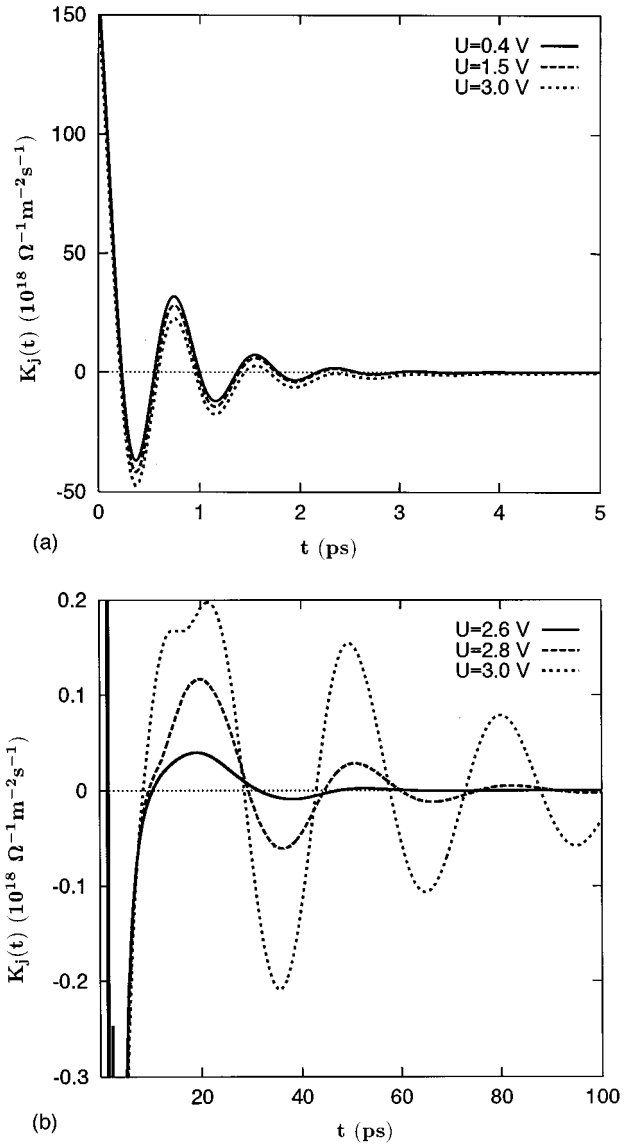

FIG. 5. (a) Short- and (b) long-time behavior of the response function of the conduction current calculated with the HD approach at several values of the applied voltage U.

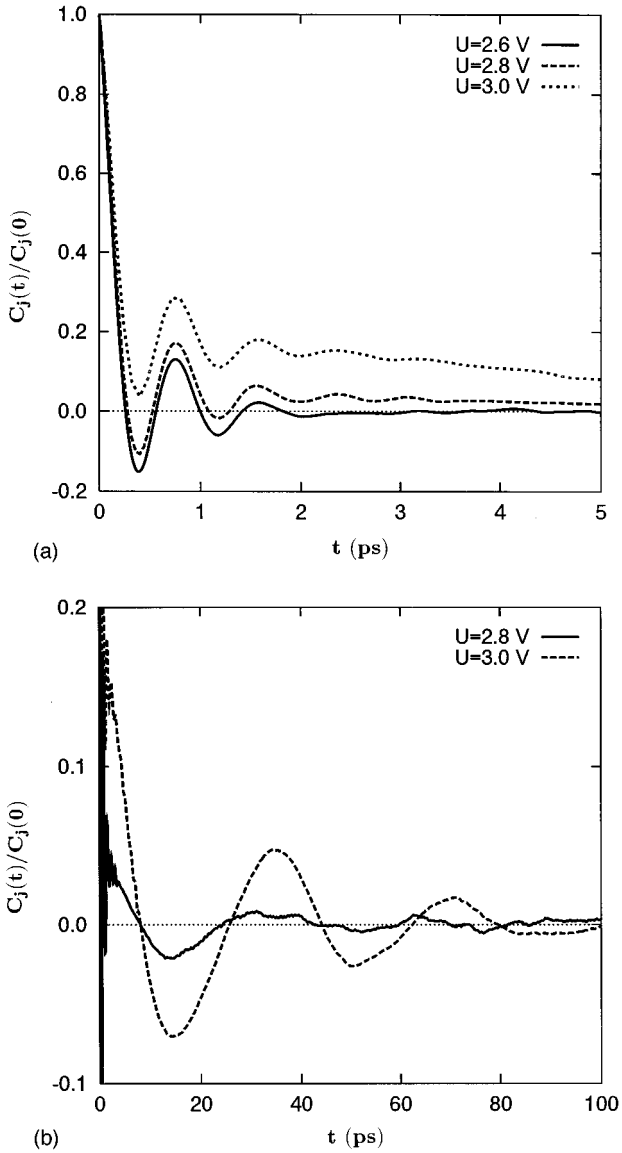

FIG. 6. (a) Short- and (b) long-time behavior of the correlation function of the current fluctuations calculated with the MCP method at several values of the applied voltage U.

threshold we observe nonvanishing self-oscillations of the current in MCP simulations as well. In this situation the oscillating tail of the correlation function becomes too long, and the calculation of $C_j(t)$ very difficult.

The spectra of $\mathrm{Re}[Y(f)]$ and $S_j(f)$, calculated for several values of the applied voltages, are shown in Figs. 7 and 8, respectively. At low voltages ($U<1.5$ V), both $\mathrm{Re}[Y(f)]$ and $S_j(f)$ remain nearly flat up to frequencies of about 100 GHz, and then begin to decrease toward a $1/f^2$ slope. For the spectrum of current fluctuations this behavior is analogous to that of velocity fluctuations in a homogeneous structure when carrier heating is accounted for. A plasma peak similar to that at thermal equilibrium is observed in the high-frequency wing of both spectra. Since electron heating in the n^+ regions is negligible, the frequency behavior of both $\mathrm{Re}[Y(f)]$ and $S_j(f)$ at the resonant peak is practically independent of the applied voltage. When the voltage approaches the threshold value, an additional resonant behavior of $\mathrm{Re}[Y(f)]$ and $S_j(f)$ caused by the transit-time effect appears in the intermediate-frequency range $f\equiv 20$–30 GHz. At $U=2.8$ V (i.e., slightly below the threshold value) negative values of $\mathrm{Re}[Y(f)]$ appear in a narrow frequency range. The decrease of $\mathrm{Re}[Y(f)]$ and its change of sign is accompanied by the appearance of a pronounced second peak in the spectrum of $S_j(f)$ at lower frequency (see Fig. 8, curves for $U\geqslant 2.8$ V). This second peak is associated with spontaneous oscillations of the current at the transit-time frequency, where the oscillations are caused by the spontaneous formation of Gunn domains and their subsequent drift through the n region. It should be stressed that, in this case, the transit-time resonance also leads to a considerable increase of the low-frequency value of $S_j(f)$. Moreover, for voltages above 2.8 V, both $S_j(f)$ and $\mathrm{Re}[Y(f)]$ exhibit a significative frequency dependence even below 10 GHz.

To show the difference between an amplifying and generating structure, Fig. 9 reports $\mathrm{Im}[Z(f)]$ and $\mathrm{Re}[Z(f)]$ calculated at $U=4$ V for the generating structure considered above (solid and dotted line, respectively), and $\mathrm{Im}[Z(f)]$ for

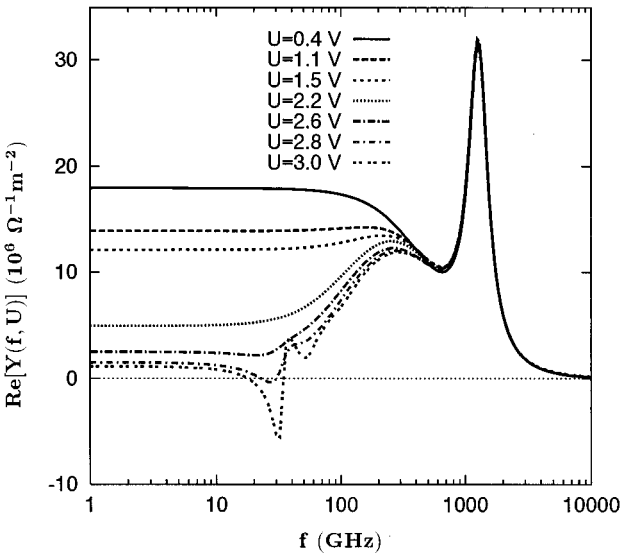

FIG. 7. Frequency dependence of the real part of the small-signal admittance for the same structure of Fig. 2 calculated by the HD approach at several values of the applied voltage U.

an amplifying n^+nn^+ GaAs structure with a lower doping of the n region: $n=2\times10^{14}$ cm^{-3} (dashed line). [For the amplifying structure $Z(f)$ has been calculated from $Y(f)$ using Eq. (13), which holds for a stable device.] For the generating structure, the spectrum of $Z(f)$ is calculated directly under current-driven operation by using the time response to a step-like variation in the total current of the voltage drop between the structure terminals.[10] (We recall that under current-driven operation the structure is always stable; i.e., it does not exhibit self-oscillations.) The main difference between the generating and amplifying structures is that, inside the amplification band (i.e., in the frequency range where Re$[Z(f)]$ is negative), Im$[Z(f)]$ of the generator becomes positive, while that of the amplifier remains negative. For the generating

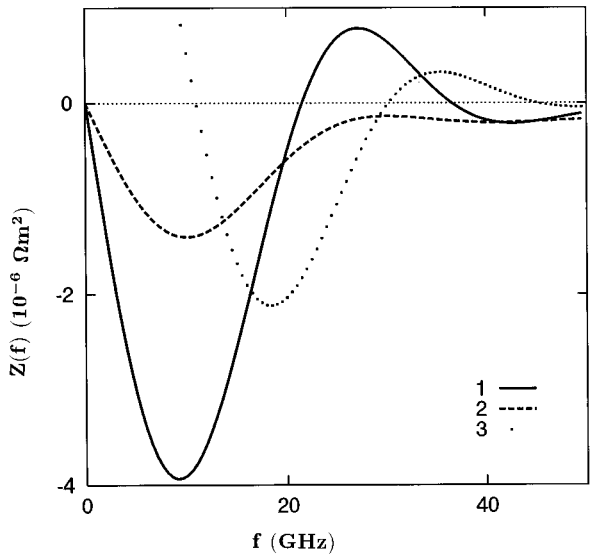

FIG. 9. Frequency dependence of the imaginary part of the small-signal impedance Im$[Z(f)]$ calculated at $U=4$ V with the HD approach for the same structure of Fig. 2 (generating device, solid line), and for a similar structure but with a lower value of the n-region doping: $n=2\times10^{14}$ cm^{-3} (amplifying device, dashed line). The dotted line refers to the real part of the small-signal impedance Re$[Z(f)]$ of the generating device.

structure considered here, the condition Im$[Z(f,U)]\geqslant0$ starts to be fulfilled inside the amplification band for $U\geqslant3.1$ V, and the structure goes to self-oscillation under constant applied voltage in the absence of an external resonant circuit. However, if the external resonant condition is satisfied, the structure can start generating even for $U\geqslant2.8$ V, when negative values of Re$[Y(f)]$ already appear but Im$[Z(f,U)]$ is still negative.

Figures 10 and 11 show the frequency dependence of

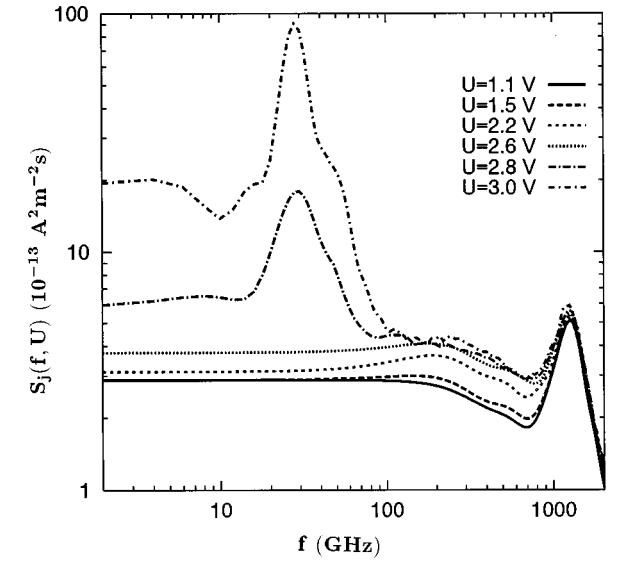

FIG. 8. Frequency dependence of the spectral density of current fluctuations for the same structure of Fig. 2 calculated with the MC method at several values of the applied voltage U.

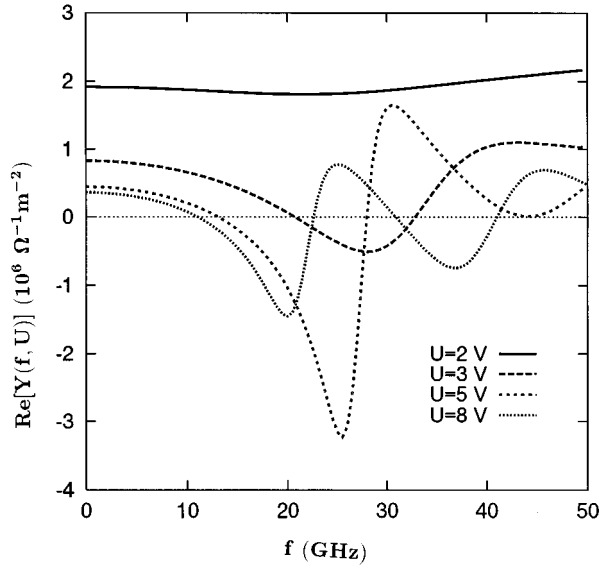

FIG. 10. Frequency dependence of the real part of the small-signal admittance for the amplifying device of Fig. 9 calculated with the HD approach at several values of the applied voltage U.

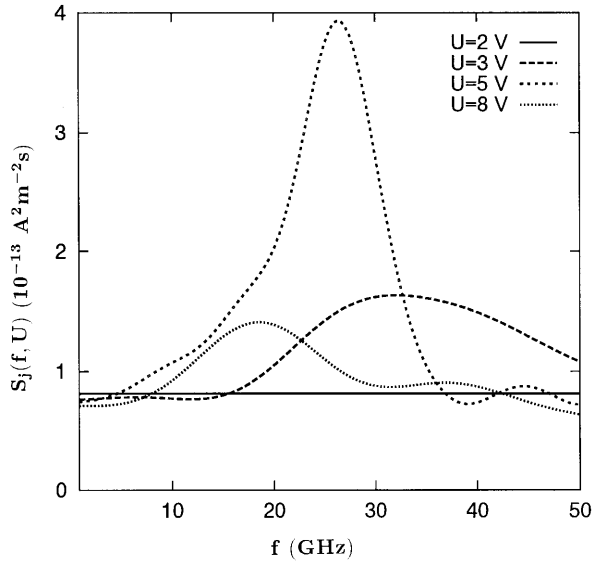

FIG. 11. Frequency dependence of the spectral density of current fluctuations for the amplifying device of Fig. 9 calculated with the MCP method at several values of the applied voltage U.

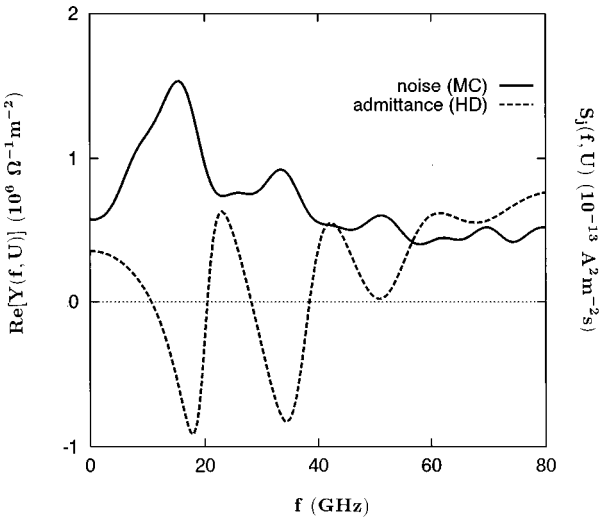

FIG. 12. Frequency dependence of Re$[Y(f)]$ and $S_j(f)$ calculated for the amplifying device of Fig. 9 with $U=10$ V.

Re$[Y(f)]$ and $S_j(f)$, respectively, calculated for the amplifying Gunn device (i.e., for the structure with $n=2\times10^{14}$ cm^{-3}). Similar to the generating structure, negative values of Re$[Y(f)]$ appear near $U=3$ V. Then, these negative values are maxima at $U=4$–5 V, and tend to decrease with a further increase of U. The amplification band is shifted to a lower-frequency range when U increases. This behavior reflects a decrease of the transit-time frequency and average velocity due to an increase of the electron transfer from the central to the upper valleys at higher electric fields. However, there appears an additional amplification band corresponding to the second harmonic of the transit-time resonance. In accordance with the admittance spectrum, the peak in $S_j(f)$ associated with the resonance at the transit time appears near $U=3$ V, reaches a maximum for $U=4$–5 V, and decreases with a further increase of U by simultaneously shifting to lower frequencies. Contrary to the case of generation, the appearance of the resonant peak does not lead to an increase of $S_j(f)$ in the low-frequency range, where it remains practically independent of the applied voltage, or even slightly decreases above the threshold value. It should be emphasized that each local minimum of Re$[Y(f)]$ leads to a separate local maximum of $S_j(f)$. This behavior is shown in Fig. 12, which presents the spectra of $S_j(f)$ and Re$[Y(f)]$ calculated for the amplifying structure at $U=10$ V.

The noise-temperature spectrum, calculated in accordance with Eq. (19) using the results of the generating structure presented in Figs. 7 and 8, is shown in Fig. 13. At low voltages, below 0.4 V, $T_n(f)$ is practically independent of the frequency, and equals the lattice temperature, thus fulfilling the Nyquist theorem. Then a systematic increase of $T_n(f)$ with U is observed. We remark that for frequencies near and above the plasma value (of about 1.3 THz) within the numerical uncertainty, we have found $T_n \simeq T_0$ at all applied voltages. This means that this part of the $T_n(f)$ spectrum is caused mainly by thermal electrons placed in n^+ regions. Thus in the following we will focus our attention on frequencies below the plasma value. In the intermediate region $0.4<U<1.5$ V, the increase of $T_n(f)$ is smooth, and mostly associated with the decrease of Re$[Y(f,U)]$. This behavior is due to carrier heating because of the high electric field inside the n region [the average value ranges between 0.5–2 kV/cm; see Fig. 4(a)]. For voltages above about 1.5 V, heating is sufficient for carrier transfer to upper valleys. Accordingly, the increase of $T_n(f)$ with applied voltage becomes more pronounced, and the spectrum exhibits a peculiar structure. The plateau at the lowest frequencies is followed by a bump evolving toward an asymptotic behavior in a small frequency region centered around the transit-time frequency $f=25$ GHz. Then, in the high-frequency range $(0.2<f<1$ THz), $T_n(f)$ flattens, taking values very similar to those of the electron temperature $T_e=2\langle\epsilon\rangle/(3k_B)$ in the n region associated with the carrier average energy $\langle\epsilon\rangle$.

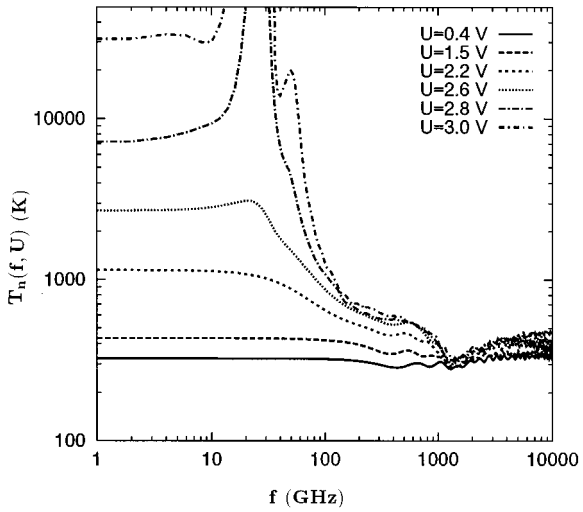

FIG. 13. Frequency dependence of the noise temperature for the generating device calculated from the admittance and noise spectra reported in Figs. 7 and 8 at several values of the applied voltage U.

From the analysis of Figs. 7, 8, and 13, we conclude that the fast increase with applied voltage of the noise temperature at the lowest frequencies is associated with both a decrease of $\mathrm{Re}[Y(f)]$ and an increase of $S_j(f)$. For voltages up to 2.6 V, the increase of $S_j(U)$ plays a minor role when compared with the decrease of $\mathrm{Re}[Y(U)]$, while above 2.6 V the increase of $S_j(U)$ also becomes quite significant. Then, due to the resonant behavior of both $\mathrm{Re}[Y(f)]$ and $S_j(f)$, there appears the bump of $T_n(f)$ near the transit-time frequency. This bump quickly goes to infinity and, according to what is discussed in Sec. II C, the noise temperature becomes negative (thus it cannot be measured) inside the amplification band $f \equiv 15-35$ GHz. At frequencies above the amplification band the noise-temperature spectrum again becomes positive (and thus measurable). For example, one can detect the second peak of the noise temperature appearing near the frequency value of 50 GHz (see curve for $U=3.0$ V) that corresponds to the second harmonic of the transit-time frequency (see the additional minimum at $f=50$ GHz of Re $[Z(f)]$ for the generating device shown in Fig. 9). Near the threshold value $U=3.1$ V (which corresponds to an average electric field of 4.2 kV/cm), the value of $T_n(f)$ at the lowest frequencies becomes practically infinity. This corresponds to the onset of electrical power self-generated at the frequency of about 25 GHz. Above this threshold voltage a noise temperature cannot be defined in the whole frequency range. Since the device exhibits self-oscillations, the only meaningful quantities remain (i) the power spectrum (directly measurable as $P_n(f)=\overline{\delta U^2_{Y_{\mathrm{load}}}}\mathrm{Re}[Y_{\mathrm{load}}(f)]$, $\delta U_{Y_{\mathrm{load}}}$ being the voltage fluctuations at the load admittance and bar denoting average over a cycle at the associated frequency), (ii) the efficiency, and (iii) the linewidth of the generator.[15,17,21,22,26] It should be emphasized that, below the threshold voltage, the above spectral behavior at the lowest frequencies is very similar to the usual noise temperature dependence on the electric field of the bulk material.[27]

Figure 14(a) reports the noise temperature at low frequencies as a function of the applied voltage for the generating device, which goes to self-oscillations under voltage-driven operation. Here curve 1 refers to the results of Fig. 13 at 10 GHz, which are compared with the available experimental data[2] presented by symbols. The correspondent dependence calculated[27] for a bulk material by using the HD approach developed in Refs. 13 and 28 is shown by curve 3. We have found excellent agreement between different theoretical approaches and experiments that proves the soundness of the theory developed here, and the reliability of the experiments. Furthermore, since curves 1 and 3 refer to the generating structure of Fig. 2, we conclude that the dependence on the applied voltage is caused mainly by hot-electron effects (similarly to what happens in the bulk material) rather than by transit-time effects. This conclusion is quantitatively supported by the calculations reported in Fig. 14(b), which correspond to the case of a stable steady state of an active device. Let us recall that such a stable state, corresponding to negative values of $\mathrm{Re}[Z(f)]$, is achieved in a wide voltage range under (i) current-driven operation for any value of the nl product, and (ii) voltage-driven operation for values of the nl product less than the critical one. The voltage dependence of the noise temperature for the structure of Fig. 2 calculated under current-driven operation is presented in Fig. 14(b) by curves 1 and 2 at frequencies of 0 and 10 GHz, respectively. Curves 3 and 4 refer to the amplifying structure of Fig. 9, and are calculated under voltage-driven operation at frequencies of 0 and 10 GHz, respectively. In both cases, the voltage dependence of the noise temperature differs significantly from that of bulk material. At $f=0$, $T_n(U)$ tends to saturate, while, at $f=10$ GHz, $T_n(U)$ increases due to the decrease of $\mathrm{Re}[Y(f)]$ since this frequency value is very close to the amplification band.

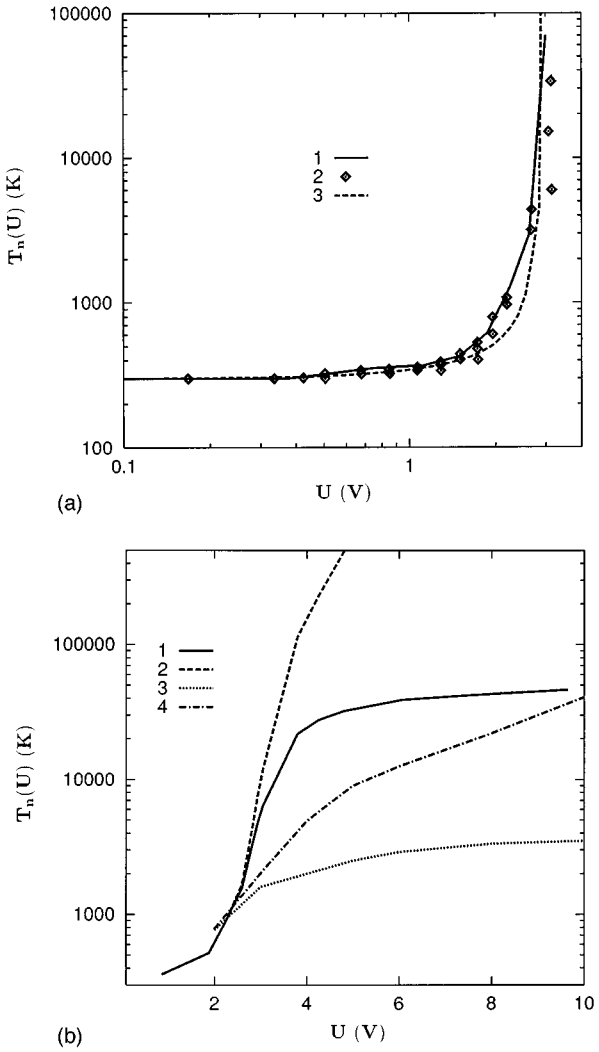

FIG. 14. Voltage dependence of the noise temperature at low frequency for (a) unstable, and (b) stable electrical behavior. (a) Symbols refer to experiments, and curve 1 to theoretical calculations performed under voltage-driven operation within MCP and HD schemes at $f=10$ GHz in the same structure of Fig. 2. Curve 3 refers to calculations performed with the balance-equation approach for bulk n-GaAs at $f=0$ (Ref. 27). (b) Curves 1 and 2 correspond to the case of current-driven operation for the same structure of Fig. 2, respectively, at $f=0$ and $f=10$ GHz. Curves 3 and 4 report calculations performed within a MCP and HD scheme for the amplifying device of Fig. 9, at $f=0$ and $f=10$ GHz, respectively.

The noise-temperature spectrum for the amplifying device is rather complicated, especially at high voltages when several amplification bands appear. Inside the amplification bands the noise measure defined by Eq. (20) can be used to

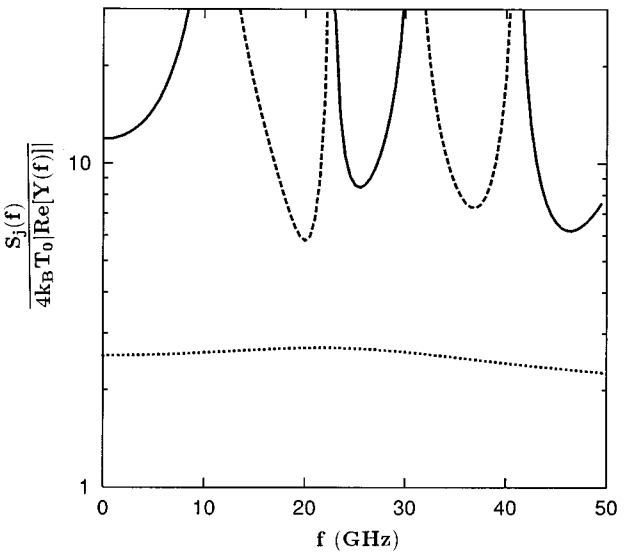

FIG. 15. Frequency dependence of the noise figure of merit. The solid line refers to the relative noise temperature $T_n(f)/T_0$, and the dashed line to the noise measure $M(f)$ defined for the amplifying device of Fig. 9 at $U=8$ V outside and inside the amplification band, respectively. The dotted line reports $T_n(f)/T_0$ calculated at $U=2$ V.

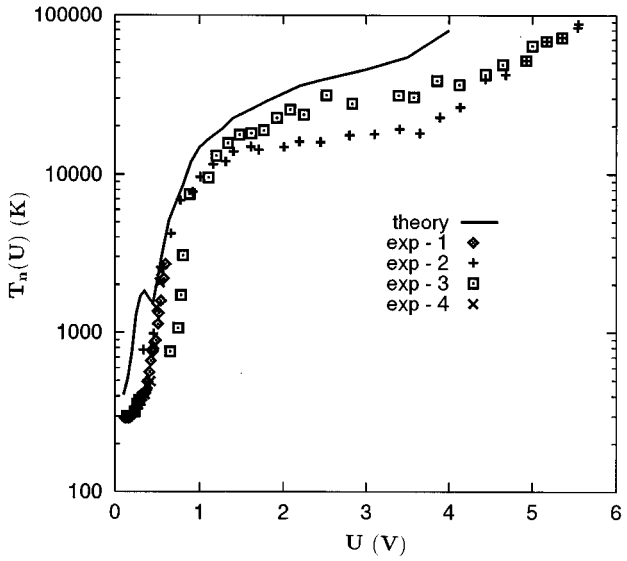

FIG. 16. Voltage dependence of the noise temperature in a submicrometer n^+nn^+ GaAs structure with the following parameters: n- and n^+-region doping of 10^{17} and 10^{18} cm^{-3}, respectively; a length of the n region of 0.2 μm; and $T_0=300$ K. Symbols refer to experiments (Refs. 2, 4, and 5), and the solid curve to theoretical calculations performed with a MCP method at $f=10$ GHz.

characterize the noise properties of the amplifier. It should be stressed that Eq. (20) is quite similar to Eq. (19), when this latter is normalized to T_0. Therefore, both $T_n(f)/T_0$ and $M(f)$ are suitable quantities to characterize the noise of the same device. The advantage is that their spectra can be plotted on the same figure, thus providing a noise figure of merit of the device operating in both the passive and active regions of the spectrum. The result of such a calculation for the amplifying structure at $U=8$ V is reported in Fig. 15. Solid and dashed curves correspond to $T_n(f)/T_0$ and $M(f)$, respectively. For comparison, the dotted curve shows $T_n(f)/T_0$ for the same device calculated at a voltage well below the threshold value.

As reported above, for the case of long structures the noise temperature at a low frequency of the stable device does not go to infinity, but even exhibits a tendency to saturate at high voltages [see Fig. 14(b), curves 1 and 3]. By scaling the length of the structure down to the submicron region, the low-frequency plateau of both $S_j(f)$ and Re$[Y(f)]$ widens to higher frequencies.[29] This opens the possibility to investigate the noise temperature in submicrometer structures, which remain stable up to sufficiently high values of the n-region doping even at applied voltages which correspond to average electric fields of several hundred kV/cm.[2,4,5] In this case, due to the wide low-frequency plateau, the noise temperature at 10 GHz is calculated from the MCP simulation directly by using, for Re$[Y(f)]$, the value obtained from the current-voltage characteristics. The results obtained for a length of the n region of 0.2 μm and a doping $n=10^{17}$ cm^{-3} and $n^+=10^{18}$ cm^{-3} are reported in Fig. 16, together with available experimental data.[2,4,5] Even if we could not extend the simulations over 4 V, the qualitative agreement between theory and experiments is considered to be satisfactory, keeping in mind that calculations are performed for a vertical rather than a planar structure as used in experiments. We remark that the absence of Gunn oscillations, typical of longer structures, makes it possible to measure T_n up to voltages of 6 V under voltage-driven operation.

IV. CONCLUSIONS

We have developed a microscopic theory of the noise temperature for n^+nn^+ GaAs structures under the application of an external voltage. A detailed analysis of the limits of validity for a consistent definition of this physical parameter in terms of current spectral density $S_j(f)$ and small-signal admittance $Y(f)$ is given. Calculations at a kinetic level have been performed, making use of an ensemble Monte Carlo simulator self-consistently coupled with a Poisson solver for the determination of $S_j(f)$, and a hydrodynamic approach for the determination of $Y(f)$. This mixed scheme combines the advantages of consistency and numerical precision for the determination of different quantities, which are obtained within an accuracy of 10% for $S_j(f)$ and of 1% for $Y(f)$. When, under voltage-driven operation, the value of the nl product is sufficiently high to observe the onset of current self-oscillations, the noise temperature at low frequency goes to infinity near a threshold voltage, as predicted by the steady-state characteristics of bulk material. For values of the voltage below threshold, the noise-temperature spectrum at high frequency shows structures which can be ascribed respectively to (i) transit-time effects ($f\simeq 25$ GHz), (ii) carrier mean energy ($0.2<f<1$ THz), and (iii) plasma-time effects ($f>1$ THz). A noise figure of merit displaying the behaviors of both the amplifying and generating structures has been provided. The electrical behavior of the generating structure remains stable under current-driven

operation. For this operation-mode case, and for the amplifying structure under voltage-driven operation, the noise temperature at low frequency remains finite in magnitude at voltages well above the threshold value for the Gunn effect. This behavior is spectacular in the case of submicrometer structures which remain stable up to sufficiently high values of n-region doping even at applied voltages, which corresponds to average electric fields of several hundred kV/cm.[2,4,5] For both micrometer and submicrometer structures, we found a good agreement between the theoretical calculations and experimental results available from the literature. We believe that a knowledge of the noise-temperature spectrum is an important tool, which provides useful information in a compressed form about the noise and transport properties of semiconductor two-terminal structures under far-from-equilibrium conditions.

ACKNOWLEDGMENTS

This work has been performed within the European Laboratory for Electronic Noise (ELEN), and supported by the Commission of European Community through Contract No. ER-BCHRXCT920047 and PECO Project EAST ELEN ERBCIPDCT940020. Partial support from the Italian Ministero dell'Universitá e della Ricerca Scientifica e Tecnologica (MURST), a GAAS-NET 95.01137.CT02 contract from the Italian National Research Council (CNR), and a NATO Networking Infrastructure Grant No. 951009 are gratefully acknowledged.

[1] J. P. Nougier, in *III-V Microelectronics*, edited by J. P. Nougier (Elsevier, Amsterdam, 1991), p. 183.

[2] V. Bareikis, J. Liberis, I. Matulioniene, A. Matulionis, and P. Sakalas, IEEE Trans. Electron. Devices **ED-41**, 2050 (1994).

[3] M. de Murcia, E. Richard, J. Vanbremeersch, and J. Zimmermann, IEEE Trans. Electron. Devices **ED-41**, 2082 (1994).

[4] V. Bareikis, J. Liberis, I. Matulioniene, A. Matulionis, A. Oginskis, P. Sakalas, and R. Šaltis, in *Proceedings of the 7th Vilnius Conference on Fluctuations Phenomena in Physical Systems*, edited by V. Palenskis (Vilnius University Press, 1994), p. 217.

[5] V. Aninkevičius, V. Bareikis, R. Katilius, J. Liberis, I. Matulioniene, A. Matulionis, P. Sakalas, and R. Šaltis, in *Noise in Physical Systems, and 1/f Fluctuations*, edited by V. Bareikis and R. Katilius (World Scientific, Singapore, 1995), p. 173.

[6] *Hot-Electron Transport in Semiconductors*, edited by L. Reggiani, Topics in Applied Physics Vol. 58 (Springer-Verlag, Heidelberg, 1985).

[7] W. Shockley, Bell Syst. Tech. J. **XXXIII**, 799 (1954).

[8] R. Bosch and H. W. Thim, IEEE Trans. Electron Devices **ED-21**, 16 (1974).

[9] S. E. Laux, IEEE Trans. Electron. Devices **ED-32**, 2028 (1985).

[10] V. Gružinskis, E. Starikov, P. Shiktorov, L. Reggiani, M. Saraniti, and L. Varani, Lith. J. Phys. **32**, 169 (1992).

[11] V. Gružinskis, E. Starikov, P. Shiktorov, L. Reggiani, M. Saraniti, and L. Varani, Appl. Phys. Lett. **61**, 1456 (1992).

[12] V. Gružinskis, E. Starikov, and P. Shiktorov, Solid-State Electron. **36**, 1055 (1993); **36**, 1067 (1993).

[13] V. Gružinskis, E. Starikov, P. Shiktorov, L. Reggiani, M. Saraniti, and L. Varani, Semicond. Sci. Technol. **8**, 1283 (1993).

[14] V. Gružinskis, E. Starikov, P. Shiktorov, L. Reggiani, M. Saraniti, and L. Varani, in *Simulation of Semiconductor Devices and Processes*, edited by S. Selberherr, H. Stippel, and E. Strasser (Springer-Verlag, Berlin, 1993), Vol. 5, p. 149.

[15] V. Gružinskis, E. Starikov, P. Shiktorov, L. Reggiani, and L. Varani, J. Appl. Phys. **76**, 5260 (1994).

[16] L. Reggiani, T. Kuhn, and L. Varani, Appl. Phys. A **54**, 411 (1992).

[17] V. Mitin, V. Gružinskis, E. Starikov, and P. Shiktorov, J. Appl. Phys. **75**, 935 (1994).

[18] L. Varani, L. Reggiani, T. Kuhn, T. Gonzalez, and D. Pardo, IEEE Trans. Electron. Devices **ED-41**, 1916 (1994).

[19] R. W. Hockney and J. W. Eastwood, *Computer Simulation Using Particles* (McGraw-Hill, New York, 1981).

[20] S. Ramo, Proc. IRE **27**, 584 (1939).

[21] V. Gružinskis, E. Starikov, and P. Shiktorov, Liet. Fiz. Žurn. **34**, 254 (1994).

[22] V. Gružinskis, E. Starikov, P. Shiktorov, L. Reggiani, M. Saraniti, and L. Varani, in *Simulation of Semiconductor Devices and Processes* (Ref. 14), p. 333.

[23] B. C. DeLoach, IRE Trans. Electron Devices **ED-9**, 366 (1962).

[24] H. K. Gummel and J. L. Blue, IEEE Trans. Electron Devices **ED-14**, 569 (1967).

[25] K. Brennan and K. Hess, Solid-State Electron. **27**, 347 (1984).

[26] V. Gružinskis, E. Starikov, P. Shiktorov, R. Gricius, V. Mitin, L. Reggiani, and L. Varani, Semicond. Sci. Technol. **9**, 1843 (1994).

[27] E. Starikov, P. Shiktorov, V. Gružinskis, L. Reggiani, L. Varani, J. C. Vaissiere, and J. P. Nougier, Lith. J. Phys. **35**, 408 (1995).

[28] L. Varani, J. C. Vaissiere, J. P. Nougier, P. Houlet, L. Reggiani, E. Starikov, P. Shiktorov, V. Gružinskis, and L. Hlou, in *Noise in Physical Systems and 1/f Fluctuations* (Ref. 5), p. 217.

[29] E. Starikov, P. Shiktorov, V. Gružinskis, L. Varani, J. C. Vaissiere, J. P. Nougier, and L. Reggiani, J. Appl. Phys. **79**, 242 (1996).